Astronomy Reports, Vol. 48, No. 5, 2004, pp. 407–417. Translated from Astronomicheskiĭ Zhurnal, Vol. 81, No. 5, 2004, pp. 447–458.

Analysis of a Solar Eruptive Event on November 4, 2001, Using CORONAS-F/SPIRIT Data

I. M. Chertok[1], V. A. Slemzin[2], S. V. Kuzin[2], V. V. Grechnev[3], O. I. Bugaenko[4], I. A. Zhitnik[2], A. P. Ignat'ev[2], and A. A. Pertsov[2]

[1] *Institute of Terrestrial Magnetism, Ionosphere, and Radio Wave Propagation, Troitsk, 142190 Russia*

[2] *Lebedev Institute of Physics, Leninskiĭ pr. 53, Moscow, 117924 Russia*

[3] *Institute of Solar-Terrestrial Physics, Irkutsk, Russia*

[4] *Sternberg Astronomical Institute, Universitetskiĭ pr. 13, Moscow, 119899 Russia*

Received October 13, 2003; in final form, November 10, 2003

Abstract—We analyze large-scale solar activity following the eruption of a very powerful, geoeffective coronal mass ejection in the 23rd solar cycle, observed at 175, 284, and 304 Å on November 4, 2001, using data from the CORONAS-F/SPIRIT telescope. In particular, we have shown that the restructuring of the magnetic field above the eruption center was accompanied by the formation of a multicomponent post-eruptive arcade, which was observed in all three bands over many hours and had an extent of the order of 0.5 $R_\odot$. Two kinds of dimmings were observed, i.e., compact dimmings on either side of this arcade and channeled dimmings along some extended features beyond the active region. The intensity in the dimmings decreased by several tens of percent. The enhanced emission observed at the top of the post-eruptive arcade can be due to energy release in the course of magnetic reconnection high in the corona at the relaxation stage of the perturbed magnetic field to a new equilibrium state with a closed configuration. It can also be due to an enhanced emission measure because of the oblique direction of the line of sight crossing both loop tops and footpoint regions. The spatial coincidence of the main dimmings in lines corresponding to different temperatures indicates that a plasma outflow from the transition region and coronal structures with opened field lines are responsible for these dimmings. Variations in the plasma temperature associated with coronal mass ejections probably play an important role for some dimmings, which appear different in different lines.

1. INTRODUCTION

It is well known (see the reviews [1–5] and references therein) that a coronal mass ejection (CME) and the associated restructuring of the magnetic field in an extensive region of the solar atmosphere are accompanied by a number of large-scale phenomena. In particular, so-called dimmings and post-eruptive arcades with lifetimes of several hours to a day are observed on the solar disk in the soft X-ray and extreme ultraviolet (EUV) after large halo-type CMEs.

Dimmings, or transient coronal holes, are regions of decreased intensity, which are formed after a CME near the eruption center and occupy a significant part of the solar disk [1, 4, 6–9]. As a rule, the locations and structures of dimmings adjacent to the eruption center coincide in lines corresponding to different temperatures. This suggests that dimmings result from the total or partial opening of coronal magnetic fields, which leads to an evacuation of material and a corresponding decrease in the intensity. Direct evidence for the outflow of material from dimmings located near the eruption center was revealed in [10] based on the observed Doppler shifts of some of the EUV lines. However, the narrow and extended channeled dimmings that are observed under the conditions of the complex global solar magnetosphere [8] can appear different in different lines, which suggests that an important role is played by plasma-temperature variations in the formation of some dimming structures [9].

A bright post-eruptive arcade frequently appears at the site of pre-existed sigmoidal (twisted) sheared structures. The arcade is formed due to the relaxation of the large-scale coronal magnetic field strongly perturbed by a CME to an equilibrium state through magnetic reconnection. The reconnection occurs in extended current sheets high in the corona. It is accompanied by prolonged energy release and the formation of a relatively simple loop system that increase in size and occasionally display features of cusplike structures [2–7, 11–15].

In recent years, dimmings and post-eruptive arcades associated with CMEs have been studied

1063-7729/04/4805-0407$26.00

mainly using soft X-ray heliograms obtained with the Yohkoh/SXT telescope [16], SOHO/EIT EUV data [17], and, to a lesser extent, TRACE data [18]. We analyze here the big eruptive event of November 4, 2001 (after 16^h UT) using data recorded in three EUV bands with the Ritchey–Chrétien (284 Å) and Herschel (175 and 304 Å) telescopes of the SPIRIT complex [19] onboard the CORONAS-F spacecraft [20]. Our choice of this event and the considerable interest in it are due to two additional circumstances. First, there were no SOHO/EIT observations at that time due to maintenance tests, while TRACE observed activity in a restricted region far from the eruption center. Second, this event is among the biggest and most geoeffective events in the 23rd solar cycle. Based on a number of its features and parameters, this event is comparable to the well known "Bastille Day" event of July 14, 2000 [21]. In addition to substantial solar phenomena (see below), this event was accompanied by an appreciable increase in the flux of high-energy particles detected by ground-based neutron monitors (GLE), a flux of protons with energies $E > 10$ MeV reaching 2×10^3 cm^{-2} s^{-1} sr^{-1} for several hours after the event and exceeding 10^4 cm^{-2} s^{-1} sr^{-1} when the interplanetary disturbance arrived at the Earth, an extreme geomagnetic storm with $D_{st} \approx -300$ nT, and a Forbush decrease in the Galactic cosmic rays detected at high-latitude stations exceeding 10% (see http://sgd.ngdc.noaa.gov/sgd/jsp/solarindex.jsp).

Section 2 presents general information about the SPIRIT telescopes and describes the observational data and reduction techniques used. Section 3 describes the situation preceding the eruptive event and some features of the event itself. Sections 4 and 5 consider the main analyzed objects—the post-eruptive arcade and dimmings. In Section 6, we discuss the results obtained and present concluding remarks.

2. OBSERVATIONAL DATA AND TECHNIQUES OF ANALYSIS

The SPIRIT complex [20] (see also the Web site http://www.xras.lebedev.ru) includes two EUV telescopes: the Herschel two-channel telescope–coronagraph, which observes at 175 and 304 Å, and the Ritchey–Chrétien four-channel telescope, which observes at 171, 195, 284 and 304 Å (similar to the SOHO EIT telescope [17] in its spectral characteristics). In addition, SPIRIT includes spectroheliographs operating at 177–207 Å and 285–335 Å and a crystal spectroheliograph operating at 8.42 Å (see the table).

The FeIX–XI coronal lines emitted by plasma with a temperature of $T_e \approx 1.5$ MK dominate at 175 ± 5 Å. The 284 ± 8 Å band contains a high-temperature ($T_e \approx 2.0$ MK) FeXV line. The 304 ± 12 Å band contains both the transition-region HeII ($T_e \approx 0.05$ MK) line and the lower-intensity coronal SiXI ($T_e \approx 1.6$ MK) line.

SPIRIT has been routinely observing the Sun starting from August 15, 2001. The observations include regular synoptic sessions with mean durations of 10–48 min performed in all spectral bands one to four times per day, as well as sessions scheduled for special programs: studies of the dynamics of active regions with a time resolution up to 10 s, observations of the solar corona to distances reaching $3R_\odot$, long-term (up to 20 days) observations in nonshadowed orbits with a resolution of 50–100 s, flare observations with a resolution of 7 s, spectroscopic observations, etc.

On November 4, 2001, SPIRIT was performing synoptic observations (12:19–12:20 UT) and carrying out observations every 5 min in several spectral channels of the 284 Å (18:38–19:04 UT), 175 Å (17:03–17:29 UT), and 304 Å (20:13–20:39 UT) bands. Note that the Herschel telescope obtained the 175 and 304 Å images synchronously withing 10 ms and an exposure time of 2 s. In addition, several images were obtained at these same wavelengths in other orbits. In particular, heliograms corresponding to 11:11 UT were obtained at both 175 and 304 Å.

According to the GOES data, an X-ray flare of magnitude X1.0 occurred from 16:03 to 16:57 UT but was not observed by SPIRIT because the satellite was in shadow. Images at 284, 175, and 304 Å were obtained four to five hours before the event, as well as four hours after the flare maximum. Despite the data, we are able to analyze long-term CME features such as post-eruptive arcade and dimmings.

For several hours after the flare, the arcade is brighter than the unperturbed portions of the disk by several orders of magnitude. To demonstrate the structure of the bright arcade and low-contrast features simultaneously in the heliograms, the corresponding images are shown on a nonlinear scale using a power function.

The dimmings are clearly visible in the difference images obtained by subtracting a heliogram preceding the event from those obtained during or after the event. The dimmings are visible as dark objects with decreased intensity. However, a simple subtraction of images, especially images separated by many hours, inevitably yields some bright and dark artifacts (false dimmings), because the structures observed on the disk are displaced due to solar rotation. To avoid this,

Spectral ranges observed by SPIRIT and excitation temperatures of solar-plasma ions emitting in these ranges [19, 20]

Channel	Spectral range, Å	Field of view, arcmin	Pixel size, arcsec	Ions	T, MK
Herschel telescope–coronagraph	175 ± 5	45×50	2.6	FeIX–FeXI	1–1.6
	304 ± 15	Corona at $(2–5)R_\odot$		HeII, SiXI	0.05, 1.6
Ritchey–Chrétien 4-channel telescope	171 ± 3	42×48	2.5	FeIX–FeX	1–1.3
	195 ± 6			FeXII	1.6
	284 ± 8			FeXV	2
	304 ± 8			HeII, SiXI	0.05, 1.6
MgXII spectroheliograph	8.418–8.423	> 60	4.2	MgXII	10
EUV spectroheliograph	177–207	> 60	5.2×93	OIV, FeIX–FeXXIV, CaXIV–CaXVII	0.3–16
	285–335		7.5×140	HeII, SiXI, FeXV–FeXVI, MgVIII, NiXVII, CaXVII	0.05–5

we use a procedure to correct for the solar rotation before the subtraction (similar to the technique of [8, 9]); namely, we rerotate the images at each wavelength to a single time prior to the event. We apply this rerotation to the entire visible hemisphere by rotating a spherical surface located at a heliocentric distance of $r \approx 1R_\odot$. This correction for the solar rotation is not ideal, since the three-dimensional structures observed in the EUV occupy some range of altitudes at larger heliocentric distances. However, our estimates show that the errors introduced by rotating the sphere with radius $r \approx 1R_\odot$ are negligible and cannot appreciably change the observed dimmings, at least for events in the central sector of the solar disk.

In addition to the SPIRIT data, we also used Hα heliograms, SOHO/MDI magnetograms [22], and Yohkoh/SXT soft X-ray heliograms. These heliograms are also used to analyze the post-eruptive arcade. These and other additional data related to the event under study, including information about the CME obtained in white light by the SOHO/LASCO coronagraph [23] and the CORONAS-F/SPIRIT heliograms can be found at the web site http://helios.izmiran.troitsk.ru/lars/Chertok/ in the form of images and movies.

3. SITUATION PRECEDING THE EVENT

The eruption occurred in the large active region AR 9684 (coordinates N06 W18) situated to the northwest of the disk center (Fig. 1a). A flocculus observed in Hα was intersected by an extended filament, FF. The SOHO/MDI magnetogram (Fig. 1b) shows a line separating the polarities of the photospheric magnetic field within the active region that corresponds to the filament. A comparison with the image obtained by the same instrument shows that the main sunspots had northern polarity and were located to the west of the filament. According to more detailed data, leading and trailing sunspots situated a small distance from each other were surrounded by a common penumbra, forming a typical preflare δ configuration. The magnetic field lines associated with the compact sunspot group probably closed on the scattered magnetic fields to the east of the filament.

The Yohkoh/SXT soft X-ray image (Fig. 1c) shows a large, high-temperature coronal arcade with a twisted (sigmoid) structure (see http://solar.physics.montana.edu/nuggets/2001/011109/011109.html). As was mentioned in the Introduction (see also [24]), such a structure is suggestive of a sheared magnetic configuration, providing evidence for stored excess energy and a high probability of eruption. A similar sigmoid structure was observed by SPIRIT in the hot Mg XII line before the event.

Figures 1d–1f present the CORONAS-F/SPIRIT heliograms obtained at 175 and 304 Å at 11:11 UT and at 284 Å at 12:19 UT, approximately four to five hours before the event. They show two brightened regions in the 175 and 284 Å coronal and 304 Å transition-region lines, which correspond to chromospheric flocculi on either side of the optical filament (line separating the field polarities). The preeruptive X-ray arcade is almost invisible in all three EUV bands, but there are compact bright knots located

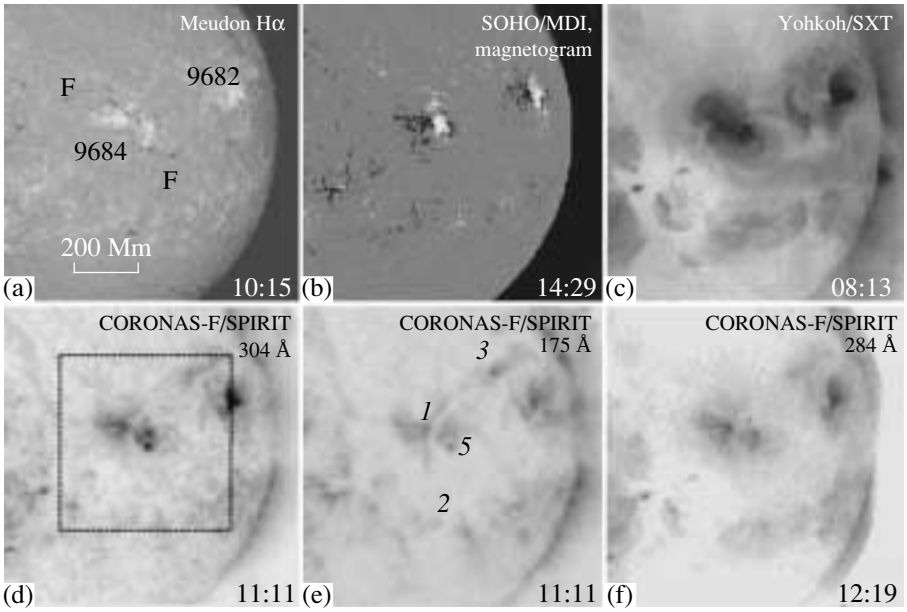

Fig. 1. Heliograms for the western disk sector illustrating the situation preceding the eruptive event of November 4, 2001. (a) Meudon Hα heliogram and (b) SOHO/MDI longitudinal magnetogram (light and dark colors correspond to northern and southern polarities, respectively). (c) Negative Yohkoh/SXT soft X-ray and CORONAS-F/SPIRIT 304, 175, and 284 Å EUV images (in order of increasing temperature).

at the ends of the central part of the arcade, which probably mark fragments of the most intense loops. In addition, there are the narrow bright (especially at 175 Å) structures 1-2 and 1-3. The first bright knot corresponds to the western edge of the bright loops bounding the X-ray arcade from the south, while the second represents a magnetic connection between the region AR 9684 and the northern neighborhood of the region AR 9682 to the west.

The event itself (Fig. 2) started with the disappearance of the southern portion of the Hα filament noted above, and included a prolonged flare of magnitude 3B/X1.0 with its maximum at 16:20 UT. The halo-type CME was observed starting from 16:35 UT with the LASCO/C2 coronagraph. The CME displayed a bright, large-scale loop structure ascending above the western limb with a high velocity in the plane of the sky ~1800 km/s. By 16:40 UT, a region of lower intensity but rapidly growing CME brightness enveloped the eastern limb sector as well, and the CME became visible around the entire occulting disk. After 17:00 UT, the CME front was visible for all positional angles of the LASCO/C3 coronagraph against an intense background of numerous protons arriving at the Earth with energies of tens of MeV (see http://cdaw.gsfc.nasa.gov/CME_list/).

4. POST-ERUPTIVE ARCADE

Figure 3 shows the post-eruptive arcade that was formed after the flare maximum observed in soft X-rays at 16:20 UT, which was detectable over many hours. The earliest CORONAS-F/SPIRIT images obtained at 304 and 175 Å at 17:03 UT (Figs. 3a and 3d) show that the most intense (i.e., dark in the negative heliograms in Fig. 3) central part of the arcade imaged in the transition region and low-temperature coronal lines consisted of a system of loops extending north–south. The brightest loops and their elements were observed at the ends of this structure (1-4 and 2-5) and also at its eastern (1-2) and western (4-5) sides. These features of the arcade, especially the predominance of the western edge, became increasingly distinct during the subsequent 26 min of observations at 304 and 175 Å (Figs. 3b and 3e). The heliograms also show the presence of some additional diffuse loops with much lower intensity to the northeast, east, and southwest of the central part of the arcade.

The heliogram obtained at 18:38 UT in the high-temperature 284 Å band (Fig. 3g) explains the multi-component structure and subsequent evolution of the arcade. We can clearly see that the brightest structure (1-4–5-2) bounds the northern and southern ends, and also the western edge of the central part of the arcade. To the south, this component of the arcade becomes a less intense but broader and more distinct system of loops (5-6–7-2). In addition, the bright loops 8-9 and surrounding halo were observed at the northern end of the arcade. The arcade component situated to the west of the bright edge 4-5 was less

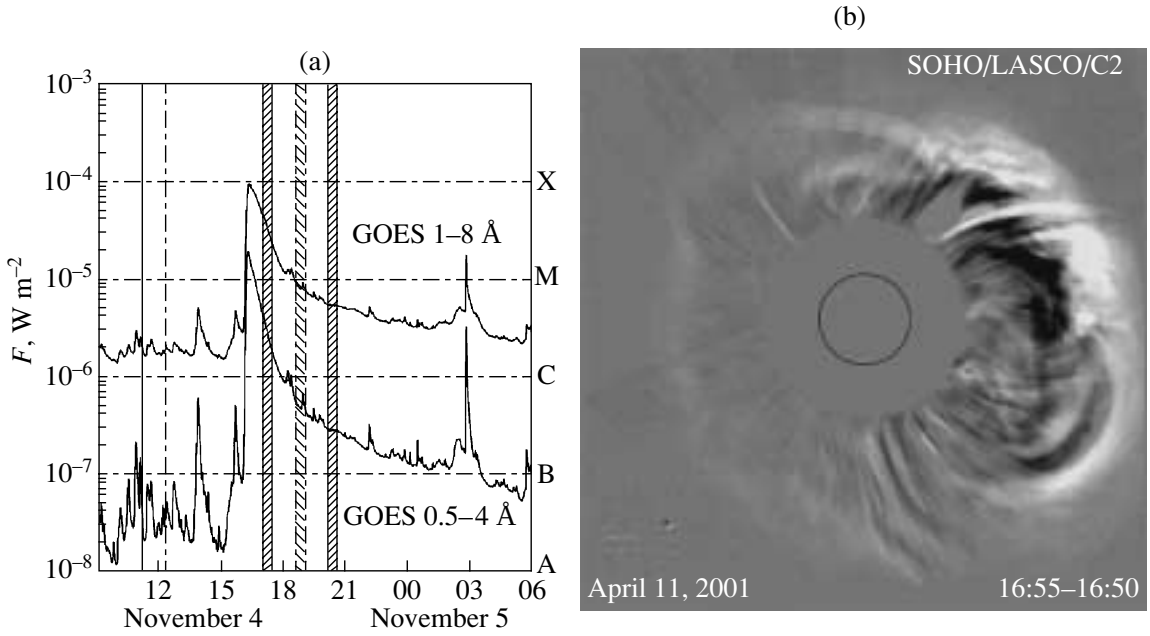

Fig. 2. (a) Evolution of soft X-ray emission detected by the GOES satellites and (b) difference CME image obtained with the SOHO/LASCO/C2 coronagraph. The vertical lines in (a) mark the times and intervals of the SPIRIT observations discussed in the text; the solid line and heavy shading mark the 175 and 304 Å bands, while the dashed line and light shading mark the 284 Å band. The central circle in (b) corresponds to the optical solar limb.

distinct. Whereas the identification of the eastern edge 1-2 with the bases of loops of the central part of the arcade seems quite obvious, there are two possible interpretations of the bright western edge 4-5: it could represent either the footpoint regions or the bright tops of loops (the so-called "spine" of the post-eruptive arcade [25, 26]).

To find an answer, we consider the Yohkoh/SXT soft X-ray image displaying high-temperature plasma with $T_e > 2.5$ MK at 18:45 UT (Fig. 3j). Along with the eastern branch (1-4) of the looplike structure, it also partially shows its western branch (4-9) at that time. We also see that its center (i.e., top 4 of this looplike structure) is the origin of the bright edge 4-5. Moreover, this edge shows a distinct southeastern extension in the form of the bright ray 5-10 passing through the central zone of the southern component of the arcade. Consequently, this suggests that both the bright edge 4-5 (observed at 304, 175, 284 Å, and in soft X-rays) and its extension 5-10 represent the bright tops of loops forming the post-eruptive arcade. Due to the observed orientation of the arcade, the "spine" in the central part of the arcade projected onto the plane of the sky may coincide with a ribbon of the western footpoints of the loops.

The subsequent arcade evolution observed in the low-temperature 304 and 175 Å bands (Figs. 3c, 3f) after 3 hours displayed a considerable decrease in the brightness of the tops of the loops of the central component of the arcade, and the extended bright structures 1-2-7 and 9-5-6 corresponding to the eastern and western footpoints of the post-eruptive loops became the most visible. Our analysis shows that the shapes and locations of these structures coincide with those for the diverging postflare Hα ribbons typical of eruptive events. The enhanced brightness at the tops of the loops in the central and southern components of the arcade was maintained over at least tens of minutes in the high-temperature 284 Å band (Figs. 3h, 3i) and over four hours in soft X rays (Figs. 3k, 3l).

Note also that the post-eruptive arcade evolved above the Hα filament and the magnetic separation line at the location of the twisted preeruptive structure (Fig. 1). The bright central component of the post-eruptive arcade was observed within the active region, while the more diffuse southern component of the arcade was observed above the zone of partial disappearance of the optical filament. The extent of the bright central part of the arcade was about 110 000–130 000 km and reached 330 000 km when the comparatively weak southern and northern components observed at 284 Å were included (Fig. 3g–3i). Such arcade lengths are typical for the largest-scale eruptive events occurring in active regions. For example, the EUV post-eruptive arcade for the Bastille Day

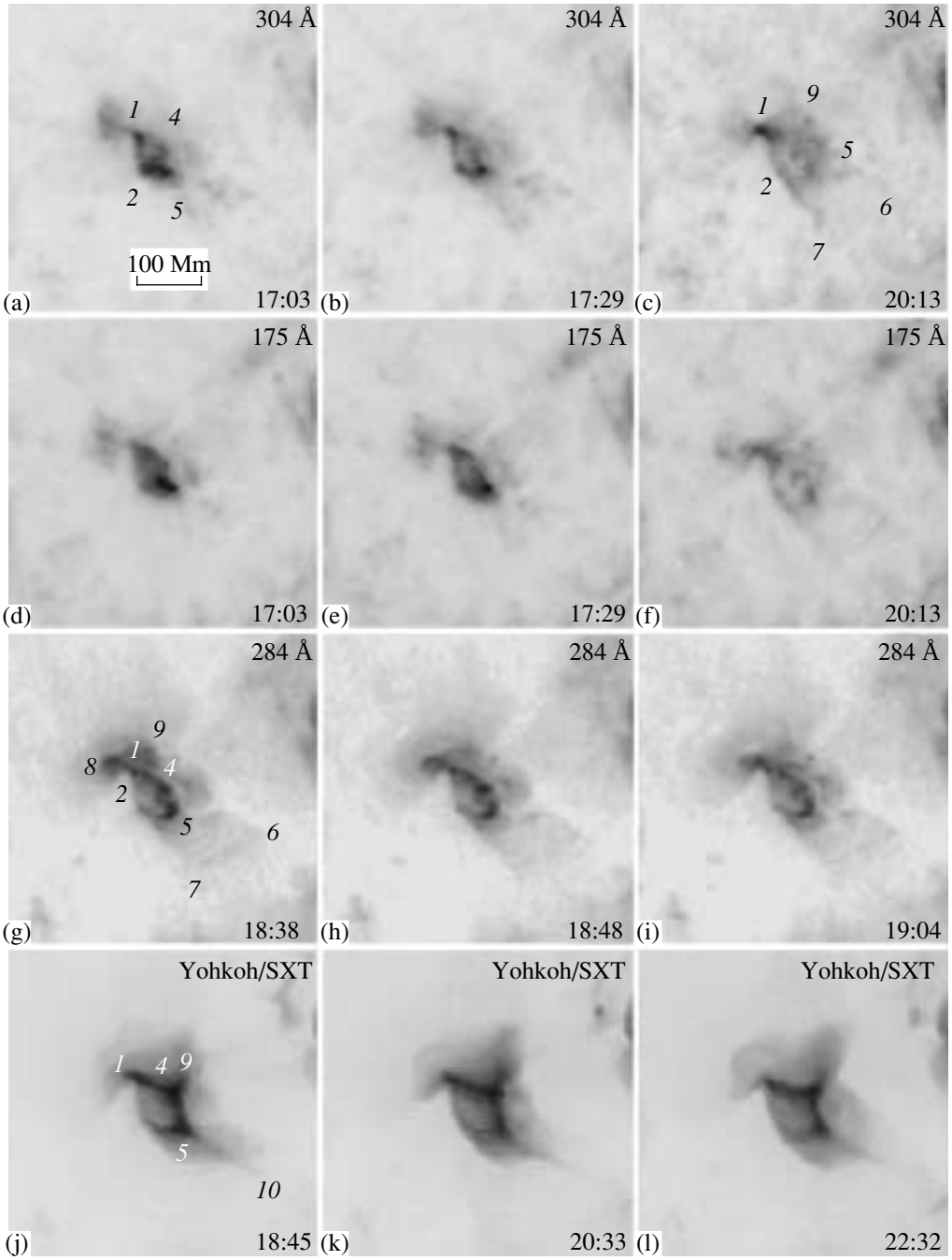

Fig. 3. Post-eruptive arcade in the negative CORONAS-F/SPIRIT heliograms obtained in the (a–c) 304 Å, (d–f) 175 Å, and (g–i) 284 Å EUV bands using the Yohkoh/SXT and (j–l) in soft X rays. All images show the area marked by the dashed frame in Fig. 1d.

event of July 14, 2000, had a total length of about 200 000 km [21].

5. DIMMINGS

The rerotated difference heliograms presented in Fig. 4 for the same western sector of the disk as in Fig. 1 illustrate the considerable size and multicomponent structure of the post-eruptive arcade. Here, the images of the central and northern components of the arcade are saturated, since the intensity thresholds were chosen for optimal representation of the dimmings accompanying the event. The images at 11:11 UT for 175 and 304 Å and at 12:19 UT for 284 Å were used as the reference preeruptive images to be compared with other heliograms obtained by the SPIRIT telescope during the event. Despite the long

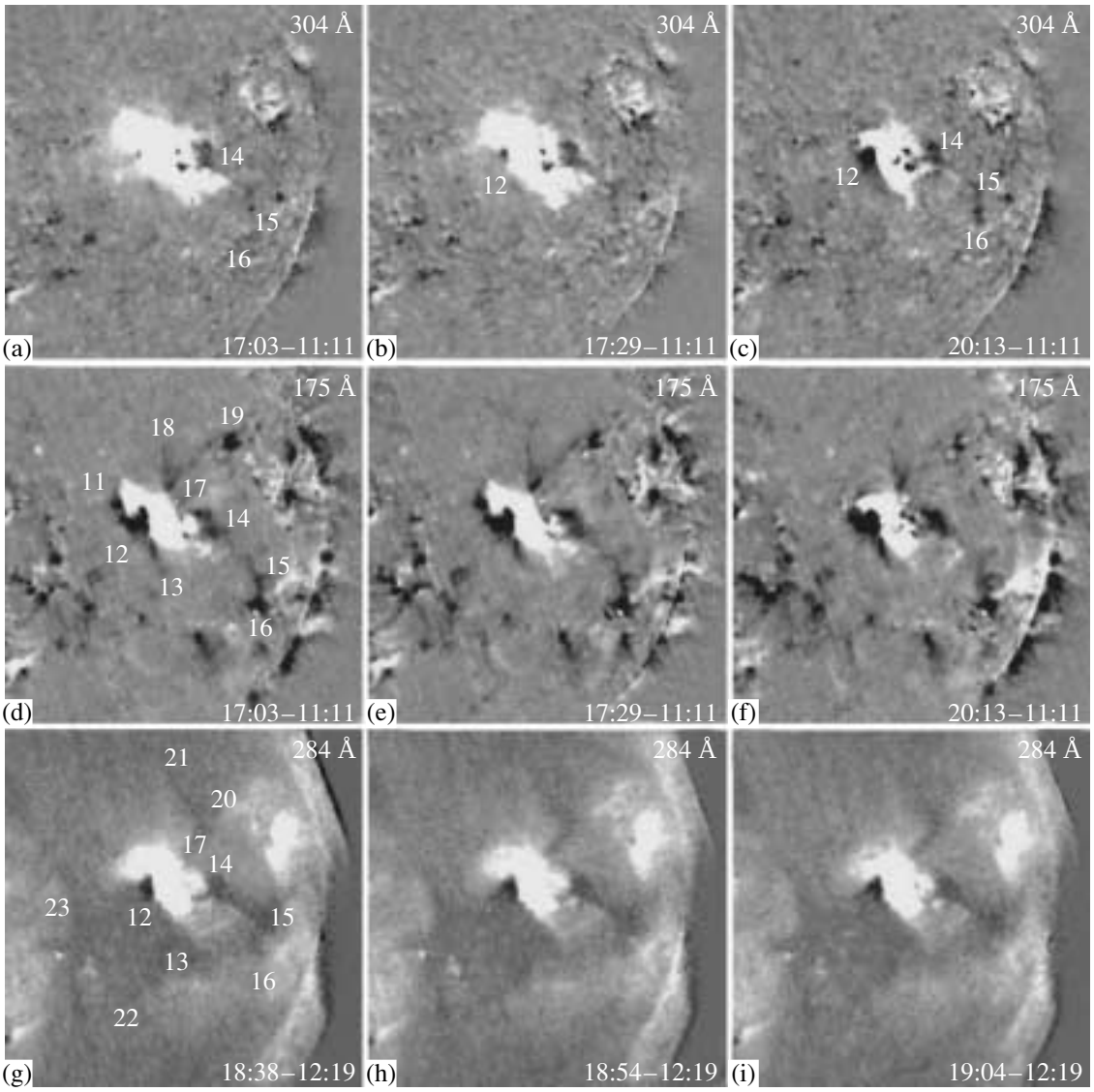

Fig. 4. Rerotated difference CORONAS-F/SPIRIT images demonstrating the bright post-eruptive arcade and dark dimmings in the (a–c) 304 Å, (d–f) 175 Å, and (g–i) 284 Å EUV bands for the same western sector of the disk as in Fig. 1.

time interval between these images and the onset of the event (four to five hours), they were chosen as the base images because there were no significant flares or eruptions on the Sun, in particular, in the western half of the disk, during this interval. Therefore, the main changes detected in the difference images of the active region AR 9684 and surrounding area can be interpreted as phenomena associated with the eruptive event analyzed. We emphasize again that, as in [8, 9], obtaining correct difference images for such a long time interval requires a preliminary rerotation of the heliograms to the same single time. In our case, the correction for the solar rotation was carried out by rerotating the heliograms to the times of the first images obtained by the SPIRIT telescope after the event maximum, namely, 17:03 UT for the images at 175 and 304 Å and 18:38 UT for those at 284 Å.

Let us start our analysis of the dimmings with the 175 Å data, since, according to [9], the most distinct dimmings are manifest in coronal lines with moderate excitation temperatures. Figure 4d, which corresponds to 17:03 UT, shows, along with the bright arcade, some persistent dark structures with intensities that are significantly lower than in the reference image. These structures are dimmings. The most prominent are the comparatively compact dimmings (11-12-13 and 14) immediately adjacent to the post-eruptive arcade at its eastern and western sides. These are accompanied by several narrow, extended channeled dimmings. One of these

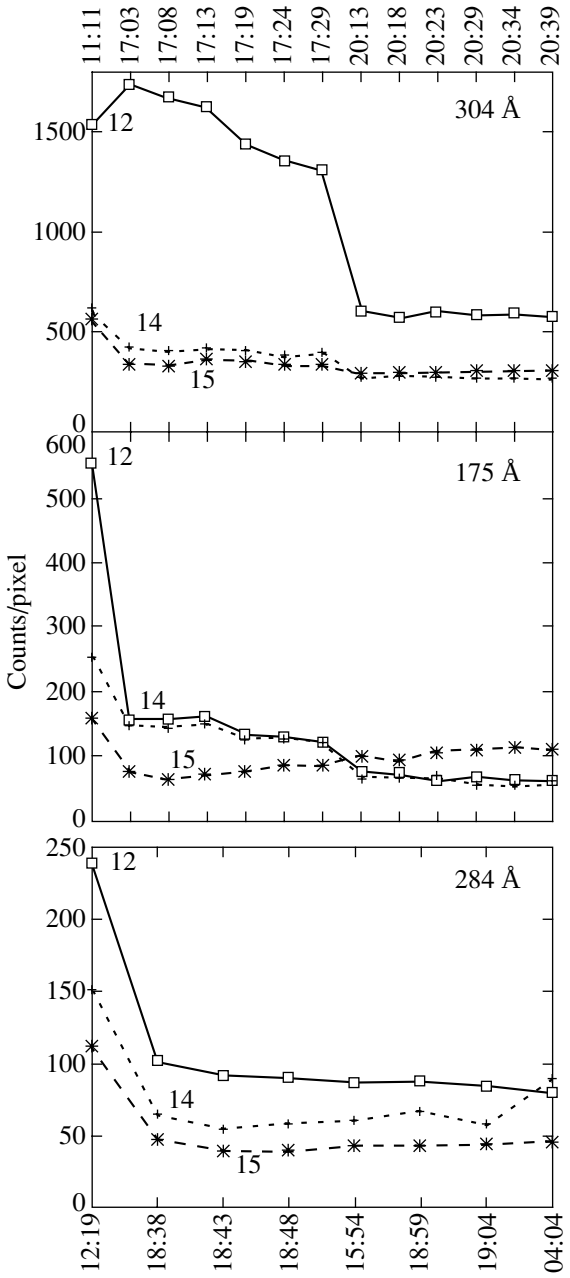

Fig. 5. Intensity variations within 22″ × 22″ areas at the centers of the main dimmings labeled in Fig. 4 by the corresponding numbers, depending on the observation times of the images.

(14-15-16) extends from the western compact dimming to the southwestern limb. Two other channeled dimmings (17-18 and 17-19) extend to the north and northwest from the dimming node at the northern end of the arcade. The length of these channeled dimmings is comparable to or greater than the extent of the post-eruptive arcade. There are other dark structures in this difference image, in particular, located some distance to the east and south of the arcade, and also near the western limb. However, they are not directly connected to the arcade, and their origin and possible relation to the event under study remain open to question. The difference heliograms for 17:29 and 20:13 UT (Figs. 4e, 4f) show that the main dimmings observed at 175 Å persisted with almost no variability over the three subsequent hours. This is true, in particular, for the compact dimmings 12-13 and 14, as well as the southwestern channeled dimming 14-15-16. The northern and northwestern dimming channels 17-18 and 17-19 became somewhat weaker, although they maintained their form and location.

With some small differences, the main dimming structures are also present in the analogous difference images for the highest-temperature band, 284 Å (Figs. 4g–4i). Here, we see the central (12) and, partially, the southern (12-13) components of the eastern dimming, while there is some brightening in place of the northern fragment of this dimming at 175 Å. At 284 Å, we can also see the western compact dimming 14 and southwestern dimming channel 14-15-16, which originates from it and passes around the southern component of the post-eruptive arcade. In place of the northwestern channeled dimmings, there is the relatively weak bent dimming structure 17-20-21. The heliograms for 284 Å also show that the transient coronal hole 12-13-22-23, which is relatively weak but extended in area, apparently adjoins the eastern compact dimming 12.

The difference heliograms for the low-temperature 304 Å band (Figs. 4a, 4b) also show the compact western dimming 14 adjacent to the arcade and, partially, the southwestern dimming channel 14-15-16. However, there is almost no sign of the northwestern channeled dimmings. The most important difference from the dimming features observed at 175 and 284 Å is that, at 304 Å, the central portion of the eastern compact dimming 12 initially displayed only a small dark element (Fig. 4a). The area of this dimming gradually increased during 17:03–17:29 UT (Fig. 4b). The dimming takes approximately the same shape and area as those observed in the earliest images at 175 and 284 Å (Figs. 4d and 4g) only until 20:13 UT (Fig. 4c). At 304 Å, the southwestern channeled dimming 14-15-16 is also the most distinct in the heliogram for 20:13 UT. Note that the dark elements visible at 304 Å within the central part of the post-eruptive arcade resulted from the fading or shifting of bright features observed in the reference heliogram for 11:11 UT (Fig. 1d).

When analyzing the heliograms for 304 Å, we should keep in mind that, in principle, the SiXI coronal line can contribute to the observed intensity variations along with the HeII transition-region line, al-

though it is obvious that the contribution of the silicon line will not dominate. The distinctions between the dimmings described above observed at 304 Å, on the one hand, and 175 and 284 Å, on the other hand, support of this statement. In addition, comparison with the preeruptive heliograms (Fig. 1) shows that it is primarily structures localized either at the very edge of or beyond the active region that were subject to dimmings as a result of the eruption. In particular, the compact dimmings 12-13 and 14, which coincided in all three bands (i.e., in all three corresponding temperatures), at least at the end of the event, were localized along the eastern edge 1-2 and southwestern end 5 of the preeruptive arcade, while the southwestern dimming channel 14-15-16 and the channeled dimming 17-19, observed mainly at 175 Å, were identified with bright structures extending from AR 9684 to the northwestern and southeastern limb sectors of the disk.

The extent of the intensity decrease in the dimmings compared to the preeruptive level, that is, the dimming depth, is presented in Fig. 5. The variations in the radiation intensity integrated over a $22'' \times 22''$ areas located in the central portion of the main dimmings labeled by the corresponding numbers in Fig. 4 are shown here for the three EUV bands. Since the time intervals between neighboring images differ widely (see Section 2 and Fig. 2), the time when the sequenced images were obtained is indicated along the horizontal axis. The curves in Fig. 5 show that the dimming depth reaches tens of percent in all three EUV bands. The channeled dimmings were somewhat shallower than the dimmings at the eruption center. The eastern (12) and western (14) compact dimmings (Figs. 5b, 5c) in the 175 and 248 Å coronal lines were the deepest (40–70%). The depth of these dimmings in the 304 Å transition-region line (Fig. 5a) is also significant (30–60%). In addition, we can see that, at 304 Å, the eastern dimming 12 appreciably lags behind the other dimmings in both area (see above) and depth. While the main decrease in the emission of the dimmings in the coronal lines and the western dimming (14) in the transition-region line was detected in the first images following the onset of the event (17:03 UT for 175 and 304 Å and 18:38 UT for 284 Å), the emission of the eastern dimming 12 at 304 Å significantly decreased between 17:29 and 20:13 UT. Figure 5 also indicates that the decreased intensities in both the coronal and transition-region dimmings were maintained over several hours.

6. DISCUSSION AND CONCLUSIONS

Our analysis of CORONAS-F/SPIRIT data at 175, 284, and 304 Å, which correspond to different temperatures, for a large-scale, geoeffective CME displays the long-term and large-scale phenomena typical of the post-eruptive phase of such events, namely, a post-eruptive arcade and dimmings.

The structure of the post-eruptive arcade provides evidence for a transition from the complex, sheared magnetic structure observed in soft X rays before the event to a topologically simpler system of hot loops with a different orientation, transverse to the extended filament passing through the active region [3]. Thus, the magnetic configuration after the eruption differs significantly from the preeruptive configuration. This represents a convincing argument in favor of magnetic reconnection. In our case, the total extent of the arcade was almost 0.5 $R_\odot$. The brightest central and northern parts were observed within the active region (i.e., in the region of strong magnetic fields), while the broad but much weaker southern component formed above the region where the filament disappeared beyond the active region. As a whole, the post-eruptive arcade was probably generated in the region of structures involved in the CME and subjected to the largest disturbances.

The loop tops rather than the footpoint regions in the post-eruptive arcade displayed the maximum brightness over several hours, especially in the high-temperature 284 Å band and in soft X rays. Similar bright arcade spines have been detected in numerous other eruptive events [12, 26]. In particular, a spine was observed between two bright ribbons corresponding to the footpoints of numerous loops constituting the post-eruptive arcade of the Bastille Day event of July 14, 2000, which occurred in the central sector of the disk [14, 15, 27]. This phenomenon is explained by heating of the plasma due to the prolonged post-eruptive energy release in current sheets high in the corona [15, 28, 29], when magnetic field lines opened or stretched in the course of CME eruption relax to a new closed equilibrium state via magnetic reconnection. The hot loops are first formed if energy release occurs in this manner. For this reason, some elements of the arcade observed in our event, i.e., its southern component in our case, are most clearly visible in the high-temperature bands. Another possible reason for the enhanced emission in the upper portion of the arcade is an increase in the longitudinal emission measure when the line of sight passes through the loop at its top. Numerous observations of limb events with distinct brightening at loop tops (see, for example, [30]) support this possibility. For the location and orientation of our arcade, the lines of sight passing through the upper portions of loops can also intersect the western footpoints of the loops, where the plasma density is increased due to the evaporation of chromospheric material.

Our analysis of dimmings displaying long-term and deep post-eruptive darkening was possible due to the technique of compensating for the solar rotation by forming rerotated difference images (see [8, 9]) using heliograms separated by time intervals of many hours. In this case, similar to other eruptive events occurring in the complex global magnetosphere typical of the solar maxima, there were two types of dimmings: (i) compact, clearly distinguishable dimmings adjacent to the eruption center and (ii) narrow, extended channeled dimmings passing from the eruption center to distant regions of the disk. The compact dimmings adjacent to the eruption center and some channeled dimmings observed in lines with different excitation temperatures in the 175, 284, and 304 Å bands mainly coincide in their structure and location. This suggests that these dimmings were formed from long-lived structures located on either side of the post-eruptive arcade, with its magnetic-field lines becoming either entirely or partially open during the CME. The plasma outflow from these structures along open field lines decreases the plasma density, resulting in a decrease in the intensity of the EUV emission [1, 4, 6–10]. An additional argument in favor of this model for the formation of the dimmings is that the lifetimes of dimmings are many hours and the recovery to a closed configuration is a very slow process (see, for example, [31, 32]). The behavior of individual portions of compact and channeled dimmings that appeared different in different coronal and transition-region lines may be associated with variations in the plasma temperature during the CME.

The presence of dimmings in both the coronal and transition-region lines indicates that their formation due to either the opening of magnetic field lines or plasma-temperature variations affected not only the corona but also the comparatively cool transition-region plasma. Analyzing the eastern and western compact dimmings 12 and 14, whose behavior at 304 Å was different, we can see that the involvement of the transition region in the CME process and the formation of dimmings there can occur either synchronously with associated coronal dimmings or with a considerable time delay of the order of tens of minutes.

Overall, the presence of a large-scale post-eruptive arcade and extended channeled dimmings provides evidence that the CME affected not only various magnetospheric layers above the eruption center but also more global structures, on scales significantly exceeding the size of the active region.

ACKNOWLEDGMENTS

The authors are grateful to the scientific leaders of the CORONAS-F project, especially V.N. Oraevskiĭ and I.I. Sobel'man, who supervised the project, and the team members of the DLR Remote Sensing Data Center (Neustrelitz, Germany) and IZMIRAN Cosmic Information Technology Center (Troitsk, Russia) for the observational data used in our study. The authors also thank the staffs of the Yohkoh/SXT telescope, SOHO/MDI magnetograph, SOHO/LASCO coronagraph, GOES project, and Paris-Meudon Observatory for additional data used. This work was supported by the Russian Foundation for Basic Research (project nos. 02-02-17272, 03-02-16049, and 03-02-16591) and the Federal Ministry of Industry and Science (project nos. NSh 477.2003.2 and 1445.2003.2).

REFERENCES

1. H. S. Hudson and D. F. Webb, in *Coronal Mass Ejections*, Ed. by N. Crooker, J. Joselyn, and J. Feynman, AGU Geophys. Monograph Ser. **99**, 27 (1997).
2. D. F. Webb, J. Atmos. Sol.-Terr. Phys. **62**, 1415 (2000).
3. A. C. Sterling, J. Atmos. Sol.-Terr. Phys. **62**, 1427 (2000).
4. N. Gopalswamy and B. J. Thompson, J. Atmos. Sol.-Terr. Phys. **62**, 1427 (2000).
5. H. S. Hudson and E. W. Cliver, J. Geophys. Res. **106**, 25199 (2001).
6. B. J. Thompson, S. P. Plunkett, J. B. Gurman, *et al.*, Geophys. Res. Lett. **25**, 2465 (1998).
7. D. M. Zarro, A. C. Sterling, B. J. Thompson, *et al.*, Astrophys. J. **520**, L139 (1999).
8. I. M. Chertok and V. V. Grechnev, Astron. Zh. **80**, 162 (2003) [Astron. Rep. **47**, 139 (2003)].
9. I. M. Chertok and V. V. Grechnev, Astron. Zh. **80**, 1013 (2003) [Astron. Rep. **47**, 934 (2003)].
10. L. K. Harra and A. C. Sterling, Astrophys. J. **561**, L215 (2001).
11. S. Kahler, Astrophys. J. **214**, 891 (1977).
12. J. A. Klimchuk, L. W. Acton, K. L. Harvey, *et al.*, in *X-ray Solar Physics from Yohkoh*, Ed. by Y. Uchida, T. Watanabe, K. Shibata, and H. S. Hudson (Universal Acad. Press, Tokyo, 1994), p. 181.
13. A. C. Sterling and H. S. Hudson, Astrophys. J. **491**, L55 (1997).
14. L. Fletcher and H. Hudson, Sol. Phys. **204**, 71 (2001).
15. M. J. Aschwanden and D. Alexander, Sol. Phys. **204**, 93 (2001).
16. S. Tsuneta, L. Acton, M. Bruner, *et al.*, Sol. Phys. **136**, 37 (1991).
17. J.-P. Delaboudinière, G. E. Artzner, J. Brunaud, *et al.*, Sol. Phys. **162**, 291 (1995).
18. B. N. Handy, L. W. Acton, C. C. Kankelborg, *et al.*, Sol. Phys. **187**, 229 (1999).
19. V. N. Oraevskiĭ and I. I. Sobel'man, Pis'ma Astron. Zh. **28**, 457 (2002) [Astron. Lett. **28**, 401 (2002)].
20. I. A. Zhitnik, O. I. Bougaenko, J.-P. Delaboudinière, *et al.*, in *Proceedings of the 10th European Solar Physics Meeting*, ESA SP **506**, 915 (2002).

21. *Topical Issue on the 2000 Bastille Day Flare Event*, Ed. by O. Engvold and Z. Švestka, Sol. Phys. **204** (2001).
22. P. H. Scherrer, R. S. Bogart, R. L. Bush, *et al.*, Sol. Phys. **162**, 129 (1995).
23. G. E. Brueckner, R. A. Howard, M. J. Koomen, *et al.*, Sol. Phys. **162**, 357 (1995).
24. R. C. Canfield, H. S. Hudson, and D. E. McKenzie, Geophys. Res. Lett. **26**, 627 (1999).
25. Z. Švestka and E. Cliver, in *Eruptive Solar Flares*, Ed. by Z. Švestka *et al.* (Springer, New York, 1992), p. 1.
26. A. H. McAllister, Y. Uchida, J. I. Khan, and K. Shibata, in *X-ray Solar Physics from Yohkoh*, Ed. by Y. Uchida, T. Watanabe, K. Shibata, and H. S. Hudson (Universal Acad. Press, Tokyo, 1994), p. 189.
27. I. M. Chertok, V. V. Fomichev, A. A. Gnezdilov, *et al.*, Sol. Phys. **204**, 141 (2001).
28. J. M. McTiernan, S. R. Kane, J. V. Loran, *et al.*, Astrophys. J. **416**, L91 (1993).
29. M. A. Livshits, O. G. Badalyan, and A. V. Belov, Astron. Zh. **79**, 659 (2002) [Astron. Rep. **46**, 597 (2002)].
30. P. T. Gallagher, B. R. Dennis, S. Krucker, *et al.*, Sol. Phys. **210**, 341 (2002).
31. V. G. Fainshtein, G. V. Rudenko, and V. V. Grechnev, Sol. Phys. **181**, 133 (1998).
32. S. W. Kahler and H. S. Hudson, J. Geophys. Res. **106**, 29239 (2001).

Translated by V. Badin